Int. J. Electrochem. Sci., 17 **(2022)** Article Number: 220247, doi: 10.20964/2022.02.51

International Journal of
ELECTROCHEMICAL
SCIENCE
www.electrochemsci.org

An Electrochemical Sensing Method for Aflatoxin B1 Detection Based on Pt-coordinated Titanium-based Porphyrin MOF

Dandan Meng[1,*], *Xiaolu Gan*[2] *and Tian Tian*[1]

[1] School of Medical Laboratorial Technics, Xinyang Vocational and Technical College, Xinyang, 464000, PR. China
[2] School of Tourism, Xinyang Vocational and Technical College, Xinyang, 464000, PR. China
[*]E-mail: mengdandan_dd@163.com

Received: 2 November 2021 / *Accepted:* 9 December 2021 / *Published:* 5 January 2022

Aflatoxin is extremely carcinogenic and is one of the most important factors affecting the safety of the food industry. The traditional culture method is not able to satisfy the demand for rapid and sensitive detection in modern industry due to its shortcomings such as poor sensitivity. In this work, a Pt-coordinated titanium-based porphyrin metal organic framework (Ti-MOF-Pt) was prepared for fabrication of aflatoxin B1 (AFB1) aptamer sensor. The high-specific surface area provided by MOF and excellent electrochemical property provided by Pt can enhance the sensing performance. After optimization, the proposed AFB1 aptamer sensor can exhibit a linear detection range between 0.1-75 μg/L. The detection limit can be calculated as 31 ng/L. In addition, the proposed aptamer sensor has also presented an excellent selectivity.

Keywords: Aflatoxin B1; Aptamer sensor; Methylene blue; MOF; Food analysis

1. INTRODUCTION

Aflatoxin is a class of fungal secondary metabolites with similar structure and properties produced by *Aspergillus flavus* and *Aspergillus parasiticus*, with strong toxicity, high stability, teratogenicity, and carcinogenicity, which can inhibit the body's immune process [1,2]. Among the more than 400 aflatoxins that have been found, aflatoxin B1 (AFB1) is the most dangerous carcinogen. Aflatoxin exists widely in food crops, especially in corn, peanuts, rice and nuts in the areas with high temperature and high humidity [3–5]. In 1993, the World Health Organization Agency for Research on Cancer identified AFB1 as a class I carcinogen. Thus the establishment of a rapid method for the detection of aflatoxin in food is of great significance for food safety and human health [6,7]. Currently, aflatoxin is detected by thin-layer chromatography (TLC), colloidal gold test strips, enzyme-linked

immunoassay (ELISA), fluorescence photometric method and high performance liquid chromatography (HPLC) [8,9]. In recent years, with the continuous development of modern science and technology, the application of electrochemical analysis in the detection of aflatoxin has received an increasing attention [10,11]. Electrochemical technology is of great importance in the development of rapid methods for aflatoxin detection due to their characteristics of rapid detection, low cost, and independence from the color and turbidity of the sample [12].

Electrochemical immunosensors are adopted to detect target molecules by detecting changes in electrical signals such as current, potential and resistance before and after the specific recognition effect, with the specific affinity of antigen and antibody [13]. As a semi-antigen, AF usually needs to be bound to bovine serum protein (BSA) to form a BSA-AF complex in order to bind effectively to the corresponding antibody [14]. The electrochemical immunosensor can detect AF through the specific recognition of BSA-AF by anti-AF. For biomolecular immobilization, Owino et al. [15] adopted platinum electrodes modified with polyaniline and polystyrene sulfonic acid to immobilize AFB1 antibodies, which were closed with BSA. The immune complexes following recognition of AFB1 can impede the transport of electron. The impedance analysis show that the detection limit of the sensor is 0.1 mg/L. Raquel et al. [16] adopted carbon nanotubes functionalized with G protein and IgG for the detection of aflatoxin in contaminated rice with a detection limit of 10 μg/g using G protein targeted sequestration. To further amplify the response signal, enzyme catalysis, nanotechnology and biomagnification are often applied in combination in aflatoxin electrochemical immunosensors.

Electrochemical aptamer sensor is an analytical method based on the change of electrochemical signal before and after the binding of aptamer and ligand, with nucleic acid being the molecular recognition element. At present, the research of electrochemical aptamer sensor for aflatoxin detection method has attracted a considerable attention. Dinqkaya et al. [17] prepared an impedance-based aptamer sensor based on DNA probes. The sensor was probed with thiol-modified single-stranded DNA (SS-HSDNA), which was immobilized on a gold electrode by covalently cross-linking with gold nanoparticles. The AFB1 molecule can be specifically recognized by ss-HSDNA, which increases the electron transfer impedance and enables the detection of AFB1 by the change of resistance before and after recognition. Nguyen et al. [18] prepared an aptamer sensor to detect AFB1 by immobilizing Fe_3O_4/PANI on the surface of a Pt microelectrode and APT probe on the surface of the electrode to identify AFB1. Magnetic nanoparticles were adopted as signal amplifying elements to detect electrochemical signal changes by cyclic square wave voltammetry with a linear range of 6-60 ng/L and a detection limit of 1.98 ng/L. When the aptamer sensor is applied to the detection of aflatoxin, it does not require the BSA to bind with the test substance first, which simplifies the operation steps. In addition, the aptamer has a high affinity for aflatoxin with a high sensitivity and specificity of detection.

In this work, a Pt-coordinated titanium-based porphyrin metal organic framework (Ti-MOF-Pt) was prepared by embedding single-atom Pt through strong interactions between the four pyrrole nitrogen atoms in the rigid backbone of the porphyrin. The introduction of monatomic Pt into the center of the planar porphyrin skeleton can lead to an excellent sensitivity after the immobilization of aptamer. The prepared aptamer bionic probe was adopted for detecting AFB1 with high sensitivity.

2. EXPERIMENTAL

2.1 Materials

Methyl 4-formylbenzoate, pyrrole, ethyl acetate, methylene blue (MB), $PtCl_2$, benzonitrile potassium ferricyanide, dipotassium hydrogen phosphate, potassium dihydrogen phosphate were purchased from Shanghai Maclean Biochemical Technology Co. Aflatoxin B1, aflatoxin B2, aflatoxin G1 and aflatoxin G2 were purchased from Sigma. The AFB1 aptamer was designed according to literature [19,20] (5'-GTT GGG CAC GTG TTG TCT CTC TGT GTC TCG TGC CCT TCG CTA GGC CCA CA-3').

2.2 Preparation of aptamer sensors

PtTCPP and Ti-MOF-Pt were synthesized on the basis of published work [21]. The bare GCE was polished with 0.3 μm and 0.5 μm Al_2O_3 powder in turn, and cleaned with anhydrous ethanol and distilled water for 5 min sonication. A certain amount of 0.2 mg/mL of Ti-MOF-Pt ethanol dispersion was drop coated on the GCE surface and dried naturally. The aptamer was immobilized on the Ti-MOF-Pt/GCE surface to prepare the aptamer sensor. 10 μL of the prepared 4 μM aptamer solution was taken and incubated on the electrode surface overnight. To close the vacant sites of unattached aptamer and avoid causing non-specific binding of Ti-MOF-Pt to AFB1, the electrode was closed in 1 mM MCH for 1 h and rinsed carefully with PBS. The aptamer-modified Ti-MOF-Pt/GCE electrode was immersed in 20 μM MB solution for 10 min, after which it was removed and rinsed with PBS (denoted as AP/Ti-MOF-Pt/GCE).

2.3 Electrochemical sensing

The modified electrode is reacted with different concentrations of AFB1 standard solution after 40 min, during which the target specifically binds to the aptamer (denoted as AFB1/AP/Ti-MOFs-Pt/GCE). The competitive removal of MB adsorbed on the aptamer chain leads to the change of electrical signal in the final detection, thus achieving quantitative and sensitive detection of the target. The working electrode to be detected was immersed in PBS at pH 7.4, and a differential pulse voltammetry (DPV) scan was performed between 0.1-0.5 V with a calomel electrode being the reference electrode and a platinum column electrode being the counter electrode.

3. RESULTS AND DISCUSSION

Figure 1 shows the FTIR spectrum of Ti-MOFs-Pt, which has a very broad absorption band between at 1700-700 cm^{-1}, corresponding to the porphyrin macrocyclic skeleton [22]. The peak located at 1413 cm^{-1} can be assigned to the stretching vibration of the C=N bond in the pyrrole ring, the peak located at 1598 cm^{-1} can be assigned to the vibration of the phenyl ring outside the pyrrole ring [23], the

peak located at 797 cm^{-1} can be assigned to the para-substituted benzene ring [24] and the peak located at 1704 cm^{-1} can be assigned to the C=O stretching vibration of the carboxyl group [22]. Notably, a significant decline of the NH peak (at 1025 cm^{-1}) can be observed from Ti-MOFs-Pt compared to Ti-MOFs, along with the appearance of a new Pt-N peak near 1016 cm^{-1}[25–29], indicating that a single Pt atom has been successfully implanted in the center of the porphyrin molecule.

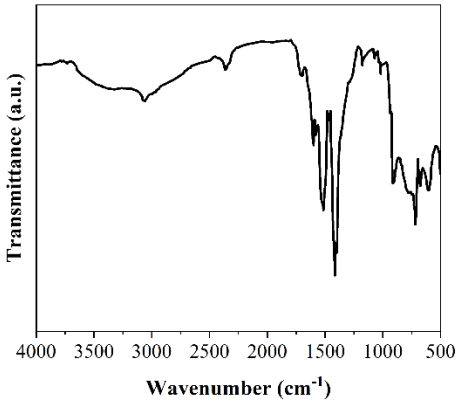

Figure 1. FTIR spectra of Ti-MOFs-Pt.

The presence of Pt can be confirmed by XPS characterization. The full XPS spectra (Figure 2A) shows that the pure Pt peak can be seen at 74.1 eV, which confirms that Pt atoms. The Pt 4f spectrum (Figure 2B) shows two peaks at binding energies of 76.5 and 73.1 eV, corresponding to the $4f_{5/2}$ and $4f_{7/2}$, respectively [30]. The peak positions between Pt(II) and Pt(0) suggest that the positively charged Pt atoms can be effectively electron-transferred through enhanced interactions between the porphyrin-linked ligand and the embedded Pt atoms [31–33].

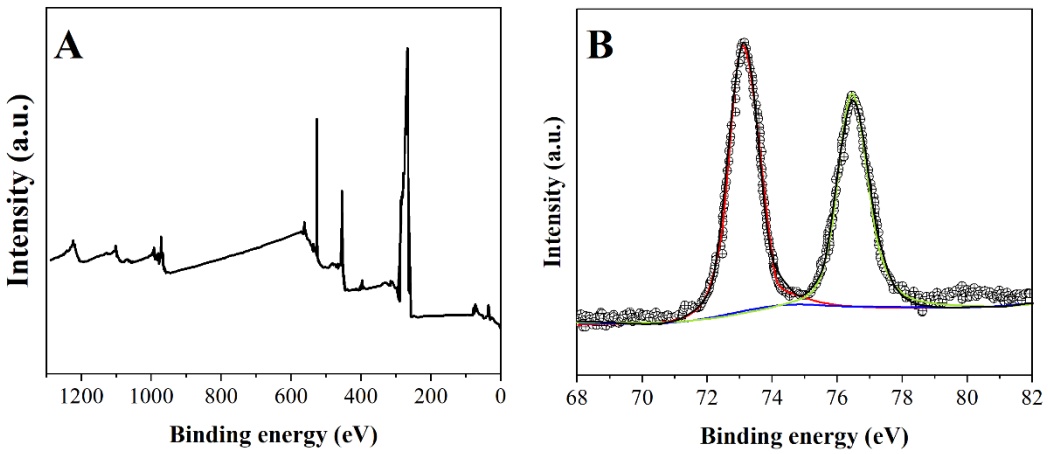

Figure 2. (A) XPS full spectrum and (B) Pt 4f spectrum of Ti-MOFs-Pt.

TEM has been adopted for observing the morphology of Ti-MOFs-Pt. As shown in Figure 3A, Ti-MOFs-Pt exhibits a multi-vacancy morphology, providing more efficient contact interfaces and exposed surface active sites [34].

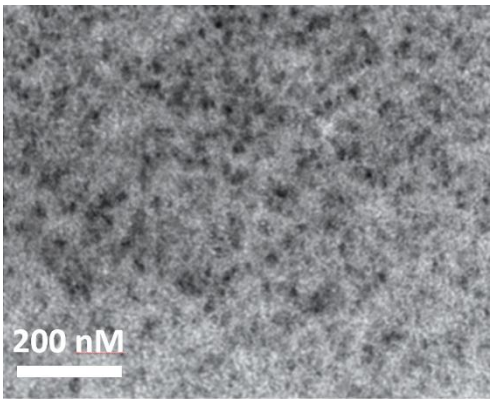

Figure 3. TEM image of Ti-MOFs-Pt.

In this experiment, CV was selected for the electrochemical characterization of the modification process of the electrode. As shown in Figure 4, the detection process was carried out in 1 mM $K_3[Fe(CN)_6]$. The CV curve of the bare GCE, marked with (a), shows that the redox reaction of the electrochemical probe $[Fe(CN)_6]^{3-}$ produces a pair of obvious redox peaks in the voltage range of -0.2-0.6 V, while (b) is the CV curve of the electrode surface modified with Ti-MOFs-Pt, and it is obvious that the peak current value increases, which presents the high-specific surface area and excellent electrical conductivity of Ti-MOFs-Pt, and also shows that the electron transfer rate of the electrode modified with Ti-MOFs-Pt is accelerated.

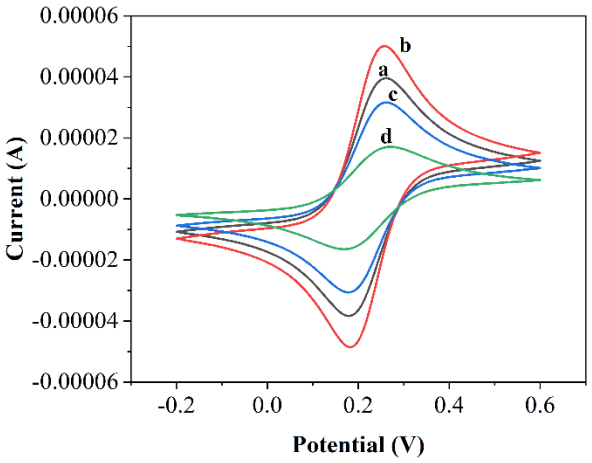

Figure 4. CV curves of bare (a) GCE, (b) Ti-MOFs-Pt/GCE, (c) AP/Ti-MOFs-Pt/GCE and (d) AFB1/AP/Ti-MOFs-Pt/GCE at 1 mM $K_3[Fe(CN)_6]$.

The CV curve of the aptamer attached to the electrode surface is the one denoted as (c), from which it can be found that the peak current value decreases significantly. The aptamer connection makes $[Fe(CN)_6]^{3-}$ less accessible to the electrode surface, leading to a decrease in the electrical signal. The CV curve after the specific binding of AFB1 to the aptamer is (d), which shows a further decrease in the peak current value, proving that the aptamer can specifically bind AFB1, and thus indicating that the sensor can achieve the detection of AFB1. From the differences in CV we can detect for different concentrations of AFB1.Electrochemical impedance spectroscopy (EIS) is an effective method to study the charge transfer at the interface between the electrode and the solution. The electrochemical behavior in the experimental process that is characterized by EIS further elucidates the electrode modification process.

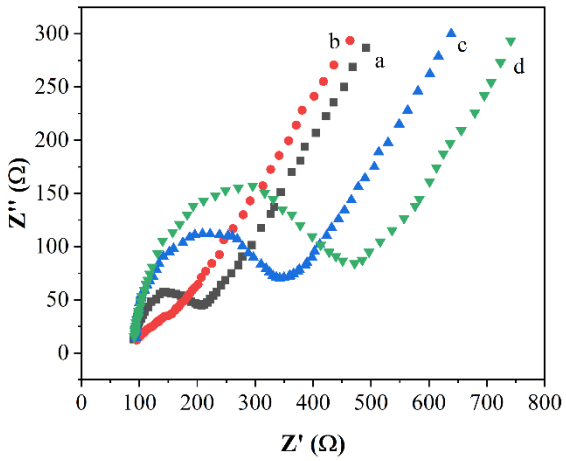

Figure 5. EIS plots of bare (a) GCE, (b) Ti-MOFs-Pt/GCE, (c) AP/Ti-MOFs-Pt/GCE and (d) AFB1/AP/Ti-MOFs-Pt/GCE in1 mM $K_3[Fe(CN)_6]$.

As shown in Figure 5, (a) shows the EIS plots of bare GCE with an impedance value of 100 Ω, while (b) shows the EIS plot after modification of Ti-MOFs-Pt. The high-specific surface area of Ti-MOFs-Pt promotes the transfer of electrons at the electrode surface, resulting in the decrease of R_{et}. Plots of (c) is the EIS after the modification of aptamer that hinders the electron transfer, leading to the increase of R_{et}, which is about 300 Ω. The EIS curve of detecting AFB1 is (d). AFB1 binds specifically to the aptamer, causing the further increase of R_{et}.

The amount of Ti-MOFs-Pt is crucial in the electrode modification process. 2, 4, 6, 8, 10, 12, and 14 μL of Ti-MOFs-Pt were selected for the electrode modification and the results are shown in Figure 6A. It can be seen in the figure that Ti-MOFs-Pt presents a significant growth of current signal in the range of 2-8 μL. The electric signal grows slowly when the drop addition volume exceeds 8 μL. With the consideration of the volumetric capacity of the electrode surface, 8 μL was chosen as the final drop addition volume.

The amount of aptamers attached is directly associated with the detection range of the constructed sensors. To ensure that a sufficient amount of aptamers were attached to the electrode surface, the concentrations of 0.5, 1, 2, 4, 6, 8 and 10 μM were selected for optimization. The results are shown in Figure 6B, which reveals that the current signal decreases sharply in the range of 0.5-4 μM. In the range

of 4-10 μM, there is only a small decrease in the current signal, thus 4 μM was chosen as the final addition concentration for the experiment.

The selection of different adsorption times of MB with aptamer also exerts an effect on the results of the sensing. The results of the assay are shown in Figure 6C. As the connection time reaches 10 min before extending the adsorption time, the amount of signal change is not significant, thus 10 min was finally selected as the adsorption time of MB with aptamer in the experiment.

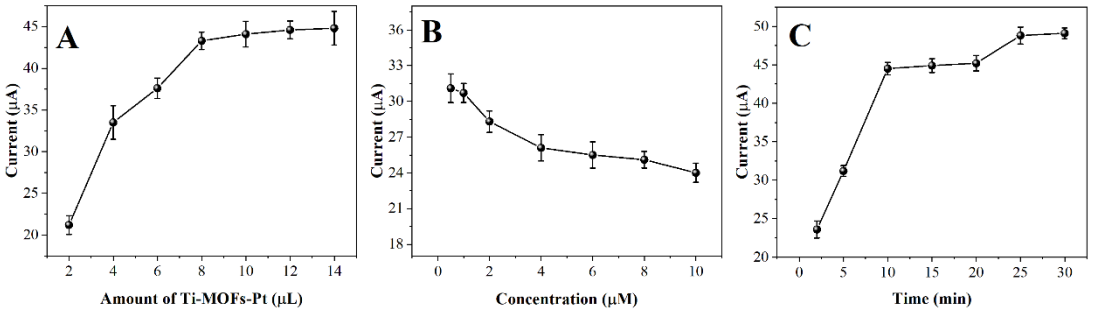

Figure 6. The effect of (A) amount of Ti-MOFs-Pt, (B) amount of aptamer, (C) MB binding time on AFB1 determination.

Under the optimal experimental conditions, different concentrations of AFB1 (0.1-80 μg/L) were selected for the DPV scan. The results are presented in Figure 7. A linear relationship between the current value and AFB1 concentration can be observed in the range of 0.1-80 μg/L. The linear regression can be found to be Current (A) = 3.58062E^{-5} Log Concentration (μg/L) -6.4791E^{-6}. The limit of detection can be calculated to be 31 ng/L. Table 1 shows the sensing comparison of the proposed AP/Ti-MOFs-Pt/GCE with other reports. It can be noted that the proposed sensor has a better performance at high concentration range.

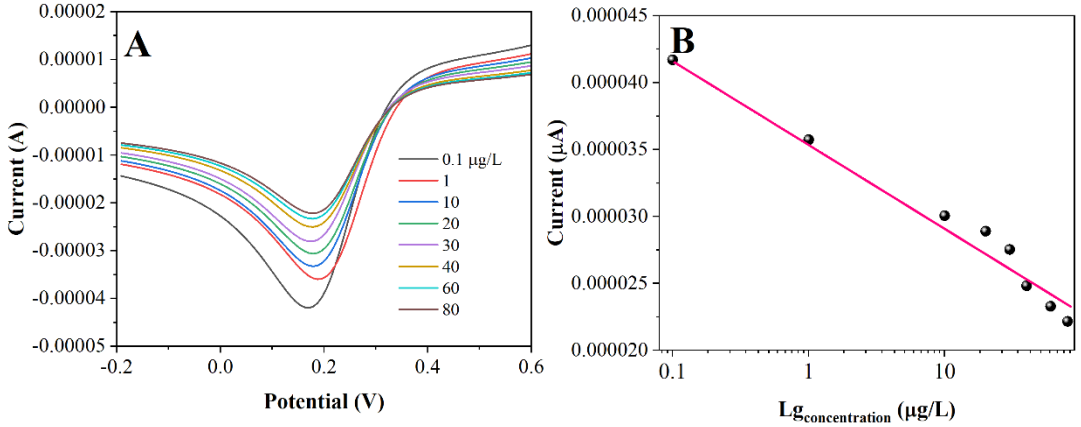

Figure 7. (A) DPV curves of AP/Ti-MOFs-Pt/GCE towards 0.1, 1, 10, 20, 30, 40, 60 and 80 μg/L of AFB1. (B) Plots of logarithm of AFB1 concentrations against the current value.

Table 1. Sensing performance of the AP/Ti-MOFs-Pt/GCE with other electrochemical sensors.

Sensor	Linear detection range	Limit of detection	Reference
Pt|PSSA|PANi|Anti-AFB1	0.1 – 0.6 ng/mL	0.1 ng/mL	[35]
GCE|Nafion|RTIL|TiO2|AuNP|Anti-AFB1-HRP	0.1 - 12 ng/mL	0.05 ng/mL	[36]
GCE|AuNP|PTH|AFB1-BSA-conjugate|HRP-blocked	0.6 - 2.4 ng/mL	0.07 ng/mL	[37]
Alkaline phosphatase (ALP)-labeled anti-mouse immunoglobulin G	0.1 to 10 ng/mL	0.04 ng/mL	[38]
AP/Ti-MOFs-Pt/GCE	0.1-75 μg/L	31 ng/L	This work

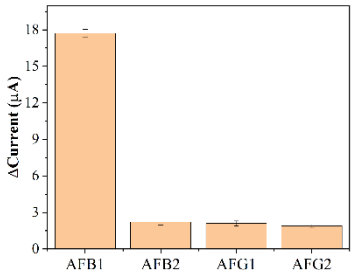

Figure 8. Selectivity of the AP/Ti-MOFs-Pt/GCE towards AFB1, AFB2, AFG1 and AFG2.

AFB2, AFG1, and AFG2 were selected as structural analogues of AFB1 for the study of sensor specificity. The same experimental method and experimental conditions were applied to the detection and three parallel experiments were conducted to obtain the results. As shown in Figure 8, it can be found that the recognition ability of the sensor for the analogues AFB2, AFG1, and AFG2 is much smaller than that of AFB1, which indicates that the constructed sensor has a good specificity for AFB1.

We selected rice and corn flour as the actual samples and performed the measurements. The samples were handled according to GB5009.22-2016. The standard addition method was used for the measurement. Table 2 shows the results of the measurements. The proposed electrochemical sensor showed an excellent performance towards AFB2 detection in both corn flour and rice. The recovery rate is between 96.05 % to 104.45 %.

Table 2. Detection of AFB2 in rice and corn flour samples using proposed electrochemical sensor.

Sample	**Addition**	**Detection**	**Recovery**
Corn flour 1	10.00 μg/L	9.77 μg/L	97.70 %
Corn flour 2	20.00 μg/L	19.21 μg/L	96.05 %
Rice 1	10 00. μg/L	10.17 μg/L	101.70 %
Rice 2	20.00 μg/L	20.89 μg/L	104.45 %

4. CONCLUSION

In this study, an electrochemical sensor was fabricated for AFB1 determination and the assembly of the aptamer sensor was characterized and optimized by CV and EIS. A linear relationship with the AFB1 concentration can be obtained in the range of 0.1-75 μg/L, while the detection limit can be calculated as 31 ng/L. The modification of Ti-MOFs-Pt increases the electrocatalytic active area of the aptamer sensor, which facilitates the amplification of the electrical signal and enables the aptamer sensor to have a wide linear detection range and a low detection limit. In future study, this methodology can also be extended for the detection of other proteins. In addition, the proposed aptamer sensor has a good specificity.

References

1. N.M. Danesh, H.B. Bostan, K. Abnous, M. Ramezani, K. Youssefi, S.M. Taghdisi and G. Karimi, *TrAC Trends Anal. Chem.*, 99 (2018) 117–128.
2. S. Akgönüllü, H. Yavuz and A. Denizli, *Talanta*, 219 (2020) 121219.
3. F.Y.H. Kutsanedzie, A.A. Agyekum, V. Annavaram and Q. Chen, *Food Chem.*, 315 (2020) 126231.
4. Z. Xue, Y. Zhang, W. Yu, J. Zhang, J. Wang, F. Wan, Y. Kim, Y. Liu and X. Kou, *Anal. Chim. Acta*, 1069 (2019) 1–27.
5. T. Sergeyeva, D. Yarynka, E. Piletska, R. Linnik, O. Zaporozhets, O. Brovko, S. Piletsky and A. El'skaya, *Talanta*, 201 (2019) 204–210.
6. A. Vaz and A.C. Cabral Silva, P. Rodrigues, A. Venâncio, *Microorganisms*, 8 (2020) 246.
7. H. He, D.-W. Sun and H. Pu, L. Huang, *Food Chem.*, 324 (2020) 126832.
8. Y. Li, D. Liu, C. Zhu, X. Shen, Y. Liu and T. You, *J. Hazard. Mater.*, 387 (2020) 122001.
9. F. Tao, H. Yao, Z. Hruska, L.W. Burger, K. Rajasekaran and D. Bhatnagar, *TrAC Trends Anal. Chem.*, 100 (2018) 65–81.
10. V. Myndrul, E. Coy, M. Bechelany and I. Iatsunskyi, *Mater. Sci. Eng. C*, 118 (2021) 111401.
11. J. Qian, C. Ren, C. Wang, K. An, H. Cui, N. Hao and K. Wang, *Biosens. Bioelectron.*, 166 (2020) 112443.
12. X. Xia, Y. Wang, H. Yang, Y. Dong, K. Zhang, Y. Lu, R. Deng and Q. He, *Food Chem.*, 283 (2019) 32–38.
13. C. Wang, Y. Li and Q. Zhao, *Biosens. Bioelectron.*, 144 (2019) 111641.
14. Z. Xu, L. Long, Y. Chen, M.L. Chen and Y.H. Cheng, *Food Chem.*, 338 (2021) 128039.
15. J.H. Owino, A. Ignaszak, A. Al-Ahmed, P.G. Baker, H. Alemu, J.C. Ngila and E.I. Iwuoha, *Anal. Bioanal. Chem.*, 388 (2007) 1069–1074.
16. R.A. Villamizar, A. Maroto and F.X. Rius, *Anal. Bioanal. Chem.*, 399 (2011) 119–126.
17. E. Dinçkaya, Ö. Kınık, M.K. Sezgintürk, Ç. Altuğ and A. Akkoca, *Biosens. Bioelectron.*, 26 (2011) 3806–3811.
18. B.H. Nguyen, L.D. Tran, Q.P. Do, H.L. Nguyen, N.H. Tran and P.X. Nguyen, *Mater. Sci. Eng. C*, 33 (2013) 2229–2234.
19. W. Zheng, J. Teng, L. Cheng, Y. Ye, D. Pan, J. Wu, F. Xue, G. Liu and W. Chen, *Biosens. Bioelectron.*, 80 (2016) 574–581.
20. F.S. Sabet, M. Hosseini, H. Khabbaz, M. Dadmehr and M.R. Ganjali, *Food Chem.*, 220 (2017) 527–532.
21. H. Feng, H. Li, X. Liu, Y. Huang, Q. Pan, R. Peng, R. Du, X. Zheng, Z. Yin, S. Li and Y. He, *Chem. Eng. J.*, 428 (2022) 132045.
22. N. Sadeghi, S. Sharifnia and M.S. Arabi, *J. CO_2 Util.*, 16 (2016) 450–457.

23. J. Ma, G. Chen, W. Bai and J. Zheng, *ACS Appl. Mater. Interfaces*, 12 (2020) 58105–58112.
24. J. Ma, W. Bai and J. Zheng, *Microchim. Acta*, 186 (2019) 482.
25. H. Karimi-Maleh, A. Ayati, R. Davoodi, B. Tanhaei, F. Karimi, S. Malekmohammadi, Y. Orooji, L. Fu and M. Sillanpää, *J. Clean. Prod.*, 291 (2021) 125880.
26. H. Karimi-Maleh, M. Alizadeh, Y. Orooji, F. Karimi, M. Baghayeri, J. Rouhi, S. Tajik, H. Beitollahi, S. Agarwal, V.K. Gupta, S. Rajendran, S. Rostamnia, L. Fu, F. Saberi-Movahed and S. Malekmohammadi, *Ind. Eng. Chem. Res.*, 60 (2021) 816–823.
27. H. Karimi-Maleh, F. Karimi, L. Fu, A.L. Sanati, M. Alizadeh, C. Karaman and Y. Orooji, *J. Hazard. Mater.*, 423 (2022) 127058.
28. H. Karimi-Maleh, A. Khataee, F. Karimi, M. Baghayeri, L. Fu, J. Rouhi, C. Karaman, O. Karaman and R. Boukherroub, *Chemosphere* (2021) 132928.
29. H. Karimi-Maleh, Y. Orooji, F. Karimi, M. Alizadeh, M. Baghayeri, J. Rouhi, S. Tajik, H. Beitollahi, S. Agarwal and V.K. Gupta, *Biosens. Bioelectron.* (2021) 113252.
30. Y. Chen, S. Ji, W. Sun, W. Chen, J. Dong, J. Wen, J. Zhang, Z. Li, L. Zheng and C. Chen, *J. Am. Chem. Soc.*, 140 (2018) 7407–7410.
31. J. Ying, Y. Zheng, H. Zhang and L. Fu, *Rev. Mex. Ing. Quím.*, 19 (2020) 585–592.
32. M. Zhang, B. Pan, Y. Wang, X. Du, L. Fu, Y. Zheng, F. Chen, W. Wu, Q. Zhou and S. Ding, *ChemistrySelect*, 5 (2020) 5035–5040.
33. L. Fu, Y. Zheng, P. Zhang and G. Lai, *Micromachines*, 12 (2021) 1048.
34. M.N. Banis, S. Sun, X. Meng, Y. Zhang, Z. Wang, R. Li, M. Cai, T.K. Sham and X. Sun, *J. Phys. Chem. C*, 117 (2013) 15457–15467.
35. J.H. Owino, A. Ignaszak, A. Al-Ahmed, P.G. Baker, H. Alemu, J.C. Ngila and E.I. Iwuoha, *Anal. Bioanal. Chem.*, 388 (2007) 1069–1074.
36. A.L. Sun, Q.A. Qi, Z.L. Dong and K.Z. Liang, *Sens. Instrum. Food Qual. Saf.*, 2 (2008) 43–50.
37. J.H.O. Owino, O.A. Arotiba, N. Hendricks, E.A. Songa, N. Jahed, T.T. Waryo, R.F. Ngece, P.G.. L. Baker and E.I. Iwuoha, *Sensors*, 8 (2008).
38. Y. Tan, X. Chu, G.L. Shen and R.Q. Yu, *Anal. Biochem.*, 387 (2009) 82–86.